ACS APPLIED MATERIALS & INTERFACES

www.acsami.org

Forum Article

Writing 3D *In Vitro* Models of Human Tendon within a Biomimetic Fibrillar Support Platform

Rosa F. Monteiro, Syeda M. Bakht, Manuel Gomez-Florit, Fernanda C. Stievani, Ana L. G. Alves, Rui L. Reis, Manuela E. Gomes,* and Rui M. A. Domingues*

Cite This: *ACS Appl. Mater. Interfaces* 2023, 15, 50598−50611

Read Online

ACCESS | Metrics & More | Article Recommendations | Supporting Information

ABSTRACT: Tendinopathies are poorly understood diseases for which treatment remains challenging. Relevant *in vitro* models to study human tendon physiology and pathophysiology are therefore highly needed. Here we propose the automated 3D writing of tendon microphysiological systems (MPSs) embedded in a biomimetic fibrillar support platform based on cellulose nanocrystals (CNCs) self-assembly. Tendon decellularized extracellular matrix (dECM) was used to formulate bioinks that closely recapitulate the biochemical signature of tendon niche. A monoculture system recreating the cellular patterns and phenotype of the tendon core was first developed and characterized. This system was then incorporated with a vascular compartment to study the crosstalk between the two cell populations. The combined biophysical and biochemical cues of the printed pattern and dECM hydrogel were revealed to be effective in inducing human-adipose-derived stem cells (hASCs) differentiation toward the tenogenic lineage. In the multicellular system, chemotactic effects promoted endothelial cells migration toward the direction of the tendon core compartment, while the established cellular crosstalk boosted hASCs tenogenesis, emulating the tendon development stages. Overall, the proposed concept is a promising strategy for the automated fabrication of humanized organotypic tendon-on-chip models that will be a valuable new tool for the study of tendon physiology and pathogenesis mechanisms and for testing new tendinopathy treatments.

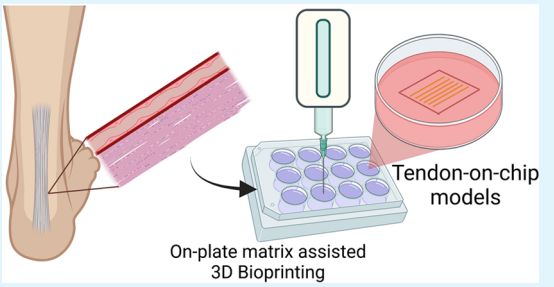

KEYWORDS: *decellularized extracellular matrix, cellulose nanocrystals, tendon-on-chip, tendinopathy, microphysiological systems*

1. INTRODUCTION

Heathy adult tendons are hypocellular tissues constituted of only 20% cells (mainly tenoblasts and tenocytes) and 80% extracellular matrix (ECM).[1,2] The ECM of this highly organized fibrous tissue is predominantly composed of fibrillar collagens, with type I being the most prevalent (≈95%), followed by type III (3%).[2] Collagen structures are surrounded by a highly viscous and hydrophilic ground substance made of proteoglycans, glycoproteins, and glycosaminoglycans (GAGs) responsible for the viscoelastic behavior of tendons, while its flexibility is provided by elastic fibers.[2,3] In tendons, collagen is hierarchically organized from the nano- to microscale into microfibrils, fibrils, fibers, and fascicles.[2] Individual fascicles are separated by a connective tissue (endotenon) that contains the blood vessels, lymphatics, and nerves, which are sheathed by the epitenon and paratenon.[4] This collagen-rich structure, known as the tendon core or tendon proper where tenocytes reside, is commonly named the intrinsic compartment of the tendon, while the extrinsic tendon compartment connects the vascular, immune, and nervous systems through synovium-like tissues.[5]

Tendon diseases, collectively named tendinopathy, are generally characterized by changes in the anisotropic organization and composition of collagen structures, increased innervation and vascularization, and persistent tissue inflammation.[6] To date, the treatment of tendinopathy remains challenging and has poor recovery outcomes.[5] New and effective treatments for these debilitating diseases and for lowering its socioeconomic burden are therefore highly needed. A main obstacle hindering consistent progress of this field is the current limited knowledge on the cellular and molecular mechanisms of tendon healing as well as on the onset and progression of tendinopathy.[4,7] Animal models have been cornerstones of preclinical research on tendon physiology, pathophysiology, and repair. However, besides being costly and low-throughput approaches and being under increasing public and ethical scrutiny with regard to animal experimentation, existing animal models cannot sufficiently emulate human tendon conditions due to inherent interspecies differences.[4,8−10] On the other hand, 2D cell culture models commonly used to study cell behavior due to their

Special Issue: Materials and Interfaces in Regenerative Medicine

Received: December 12, 2022
Accepted: March 12, 2023
Published: March 23, 2023

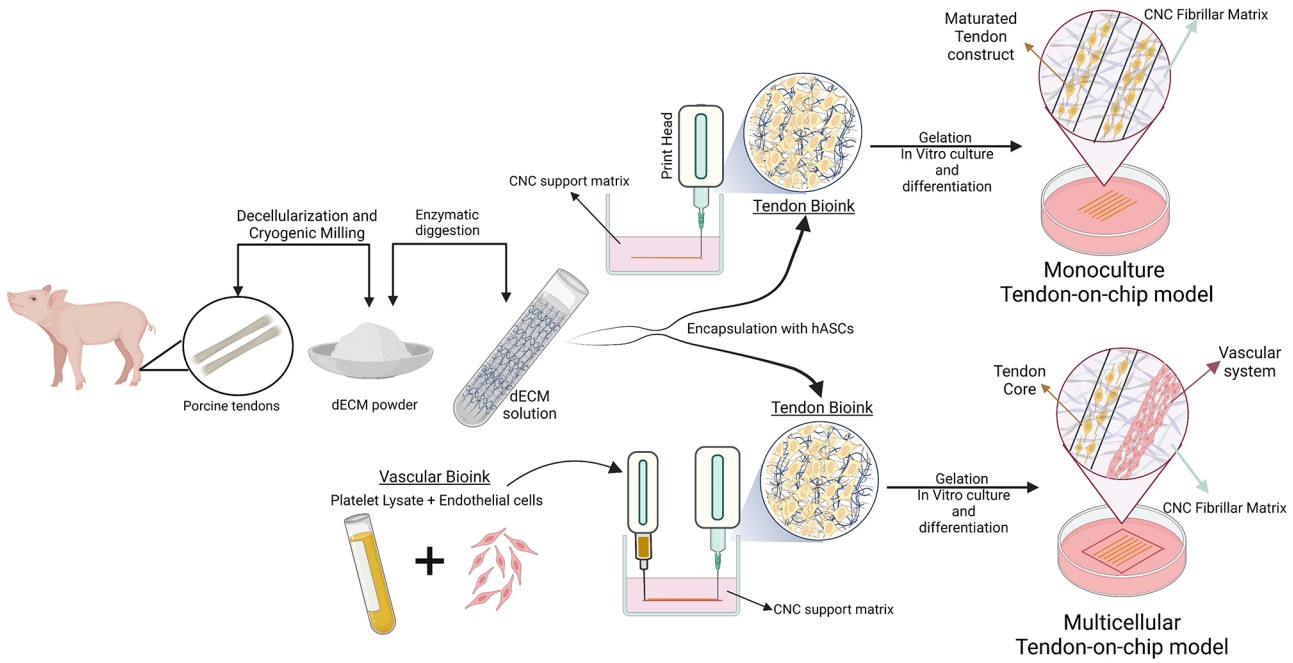

Figure 1. Schematic representation of the monoculture and multicellular tendon-on-chip fabrication process. Porcine tendons were harvested, decellularized, and milled to obtain a homogeneous dECM powder that was enzymatically digested to form the dECM ink solution. hASCs were mixed with this dECM solution and printed within CNCs support matrix to create the tendon core compartment. For multicellular systems, a square of endothelial cells bioink was printed around the tendon core to represent the vascular system. After printing, the embedded cell structures were locked within a CNC fibrillar support matrix, allowed to jellify, and cultured *in vitro*.

practicability, high-throughput, and cost-effectiveness are oversimplified systems that fail to faithfully represent the complex biophysical and biochemical cues of the native tendons' microenvironment.[4,11] Mimicking the hallmarks of tendon homeostasis and tendinopathy *in vitro* remains thus a challenging task. The development of humanized 3D *in vitro* models that can recreate the physiological context of the tissue and its repair mechanism after injury, particularly the crosstalk between tenocytes and other relevant cell populations (e.g., immune, vascular, and stem cells) under tendon-specific microenvironments, would significantly contribute to major advances this field.[8]

Bioengineered microphysiological systems (MPSs) are attractive approaches to more closely recapitulate the physiological, developmental, and disease processes of human tissues and organs *in vitro*.[12,13] One type of MPS that is gaining increased attention by the scientific community and pharmaceutical industry are organs-on-chip (OoC), dynamic systems that have been widely used for disease modeling and the testing of new drugs in preclinical stages.[14,15] Transparent biocompatible polymers such as polydimethylsiloxane (PDMS) are frequently used to fabricate the microfluidic devices in which typical OoC are built.[16] However, besides its known operational and materials-related challenges, the soft lithography microfabrication processes used for their manufacture are costly and low-throughput and have limited potential for 3D design complexity.[16,17] 3D bioprinting technologies are possible alternatives to overcoming some of the existing limitations on MPS manufacturing.[18] These automated biofabrication approaches are potentially cheaper than on-chip-based technology and allow to produce multicellular models with higher architectural complexity and biological representation.[14,19] Among them, extrusion bioprinting in suspension baths followed by its annealing/cross-linking is a manufacturing strategy that enables the direct 3D writing of different free-form MPSs housed in hydrogel materials.[20] Support baths based on self-healing or annealable granular hydrogels have been used for the direct printing of embedded multicellular systems that modeled the function of, e.g., human cardiac tissue and neuronal networks.[21,22] Similarly, our group has recently introduced a cellulose nanocrystal (CNC)-based fluid gel that can be self-assembled into a fibrillar matrix after printing, encapsulating and supporting the *in vitro* maturation of the embedded 3D constructs.[23] Overall, this system is relatively inexpensive, does not need specific microfabrication processes or equipment, and is based on a stable fibrillar matrix that allows more biomimetic cell−cell and cell−matrix crosstalk, making it an attractive platform for *in vitro* modeling.[23]

An integral component of bioprinted MPSs are the bioinks, which must be designed according to the targeted tissue or organ of interest. Although numerous hydrogel systems (e.g., based on alginate,[24] hyaluronic acid,[25] gelatin,[26] gelatin methacryloyl,[27] or collagen[28]) have been used in bioink formulations, their potential to closely mimic the native cell niche is limited.[18] Tissue- and organ-specific decellularized extracellular matrix (dECM) hydrogels are gaining increased interest in these fields because they retain the main biochemical and biophysical cues of the native tissue ECM after decellularization.[29] In particular, tendon dECM hydrogels have demonstrated the ability to induce stem-cell commitment toward the tenogenic lineage without requiring additional supplementation with biological factors, providing superior tenogenic bioactivity compared to other matrices such as collagen.[30−33] The other key components of MPSs are the selected cells for specific tissue function. Tenocytes are mature fibroblast-like cells with elongated morphology that reside along the collagen fibers and are responsible for the synthesis

https://doi.org/10.1021/acsami.2c22371
ACS Appl. Mater. Interfaces 2023, 15, 50598−50611

and continuous remodeling of the tendon ECM.[4] Although tenocytes seem to be the most obvious stroma cell source for building functional tendon MPSs,[13] the collection of tendon biopsies from healthy human donors is impracticable and the expansion of these cells *in vitro* remains challenging due to their fast phenotype drift with passaging, emphasizing the need for better alternatives.[34] One option might be the use of stromal/stem cells from easily accessible sources such as human-adipose-derived stem cells (hASCs). hASCs have been widely used in tendon engineering applications, and their differentiation toward the tenogenic phenotype can be promoted by the biophysical and biochemical cues of scaffolding biomaterials.[34,35] On the other hand, the use of hASCs in the context of tendon modeling opens the possibility for easy sourcing of patient-specific stem cells, allowing to create patient-specific preclinical models.

In this work, we propose the development of tendon MPSs by combining the concept of 3D bioprinting within suspension media with the unique niche signature of tendon dECM hydrogels for the freeform 3D writing of humanized tendon-on-chip models. For that, we successfully decellularized porcine tendons and developed a tendon dECM hydrogel, suitable for 3D bioprinting. The use of the CNCs platform allowed the printing of the desired patterns and sustain the maturation of the construct. We demonstrate the modeling potential of the concept by fabricating two versions of the tendon-on-CNC-chip of increasing complexity. A tendon core monoculture system was first developed and characterized. This system was then incorporated with endothelial cell structures to study the interaction between these two important tendon cell populations, whose roles in tendon development and disease remain poorly understood. The schematic representation of the system development can be seen in Figure 1.

2. MATERIALS AND METHODS

2.1. Porcine Tendon Decellularization and Processing. Porcine trotters were obtained from a local slaughterhouse, and the flexor *profundus* tendons were immediately harvested under aseptic conditions, following a previously optimized harvesting protocol.[36] After dissection, the tendons were cut into small pieces and frozen at −80 °C for further decellularization. The decellularization procedure followed the protocol proposed by Toprakhisar et al.[37] with some modifications. In general, this process consisted of successive washing cycles performed under sterile conditions and in an orbital shaker at 4 °C, unless otherwise indicated. Tendons were first subjected to five cycles of freeze−thaw in liquid nitrogen and phosphate-buffered saline (PBS; Sigma-Aldrich) at 37 °C, respectively, and then incubated in a solution of 50 mM tris(hydroxymethyl)aminomethane (Tris)/1.5 M NaCl (Sigma-Aldrich; pH = 7.6) overnight. The tendons were then incubated at 37 °C in a solution of 0.5% (v/v) trypsin/5 mM ethylenediaminetetraacetic acid (EDTA; Sigma-Aldrich; in PBS, pH = 7.6) and finally placed in a 2% sodium dodecyl sulfate (SDS; Sigma-Aldrich) + 2% Triton X-100 (Sigma-Aldrich) solution (w/v and v/v, respectively, in PBS) for 2 days. The tendons were rinsed with PBS and then incubated in 10 mM Tris + 1% Triton X-100 for 1 day. Next, samples were incubated in DNase (200 U/mL; VWR) at 37 °C overnight and finally washed with PBS containing antibiotic for 1 week to remove any remaining detergent or enzyme.

After decellularization, the tendons were freeze-dried and milled in a cryogenic grinder (SPEX SamplePrep) for 2 min with a rate of 20 cycles/s, resulting in a homogeneous powder of porcine tendon dECM. The dECM was then stored at −20 °C until further use.

2.2. Characterization of the Tendon dECM. To measure the double-stranded DNA (dsDNA) for DNA quantification, both native and decellularized tendon pieces were freeze-dried and then cryogenically milled as previously described, to obtain a homogeneous powder. The powder was digested for 6 h at 56 °C with proteinase K, and the remaining DNA extraction was performed using DNeasy blood and tissue kit (Qiagen) according to the manufacturer's instructions. Each sample (n = 3) was derived from different decellularization batches and weighed before the digestion step. The extracted DNA was measured using a Nanodrop spectrophotometer (Thermo Fisher Scientific).

Histology and immunohistochemistry methods were applied to fully characterize the dECM tissue, using the native tissue as the control. Native and decellularized tendon tissues were first fixed with a 10% (v/v) neutral buffered formalin solution (Thermo Fisher Scientific) for 48 h at room temperature (RT). Then, the tissues were embedded in paraffin and sectioned into 5-μm-thickness sections using a microtome. The sections of native and decellularized tissues were deparaffinized, rehydrated, and then stained with different dyes. Hematoxylin and eosin (H&E; ThermoScientific) and 6-diamidino-2-phenylindole (DAPI; VWR) staining were used to assess the efficiency of nuclear material removal by the decellularization process. Masson's Trichrome (MT; Bio-Optica) and Alcian Blue (AB; Sigma-Aldrich) were used to analyze preservation of the collagenous and GAGs content after decellularization, respectively. Finally, Sirius Red Picrate (SRP; Bio-Optica) was used to stain collagen type I and III fibrils. The H&E, AB, and MT samples were observed under an optical microscope, DAPI under a confocal microscope, and SRP under a polarized light microscope.

2.3. Production and Rheological Characterization of the dECM Hydrogel. The bioink hydrogel was prepared by subjecting the dECM powder to the typical process of enzymatic digestion in acidic conditions.[38] To evaluate the impact of the decellularization process on the cell viability (see the assay description below), 2.0% (w/v) dECM was first digested for 72 h with 1 mg/mL pepsin (P7012, Sigma-Aldrich) in a 0.02 M hydrochloric acid (HCl) solution. To evaluate the impact of the matrix concentration and degree of digestion in the rheological properties of the bioink, two different concentrations and digestion times were tested: 1.0 and 2.0% (w/v) dECM digested for 48 and 72 h with 1 mg/mL pepsin (P7012, Sigma-Aldrich) in 0.02 M HCl. After digestion, the hydrolyzed dECM was neutralized with 200 mM NaOH (PanReac) and 10× PBS in proportions of 1:10 and 1:9 of the volume, respectively, under cooling in an ice bath. To confirm its gelation ability, the neutralized matrix was incubated at 37 °C for 15 min.

The rheological properties of the precursor solutions and resulting hydrogels at concentrations of 1.0 and 2.0 wt % and subjected to 48 and 72 h of digestion were assessed using a Kinexus Pro rheometer (Malvern Instruments, U.K.). All of the measurements were performed with a parallel-plate geometry using a 20-mm-diameter plate, 1 mm gap size, and 320 μL of each precursor solution. The shear viscosity was measured in response to the shear rate from 0.001 to 100 s^{-1}, and the temperature was set to 4 °C to recreate the bioprinting conditions. After incubation at 37 °C for 30 min, in order to allow gelation of the dECM hydrogel, the frequency-dependent oscillatory shear rheology was determined by varying the frequency between 0.01 and 100 Hz (n = 3 for all rheological measurements). Mineral oil (Fisher Scientific) was used around the plate as a solvent trap to prevent water evaporation from the dECM hydrogel.

2.4. Preparation of CNC Support Media for Bioprinting. The colloidal suspension of CNCs was produced by acid hydrolysis of microcrystalline cellulose (MCC; Sigma-Aldrich), following our previously established protocol.[23,39] Briefly, sulfuric acid (95−98% from Honeywell) was added to MCC to achieve a final concentration of 62 wt % in the aqueous solution of MCC. The reaction was performed under continuous stirring at 60 °C for 40 min at 500 rpm and was stopped by adding an excess (5 times the initial volume) of cold water. After decanting, the supernatant was discarded and the remaining suspension was centrifuged (5810R, Eppendorf, Germany) for 10 min at 8603g and 5 °C until the supernatant became turbid. The resulting suspension was collected and dialyzed using a cellulose dialysis tubing membrane (MWCO = 12−14 kDa, 0−76 mm width, Sigma-Aldrich) against deionized water until neutral pH. The dialyzed

https://doi.org/10.1021/acsami.2c22371
ACS Appl. Mater. Interfaces 2023, 15, 50598−50611

suspension was removed from the membranes and subjected to five sonication cycles of 5 min (VCX 750, Sonics) using an ultrasound probe (Horn $^1/_2$-in. REPLACEABLE VCX 750, 630−0220) at 60% amplitude output and under ice cooling to prevent overheating. Then, the suspension was centrifuged one more time for 10 min at 8603*g* and 5 °C to remove any possible big particles that remained. The supernatant was collected and further degassed with a vacuum pump. The final supernatant containing CNCs was stored at 4 °C until further use, and its concentration was determined by gravimetric analysis.

To prepare the CNC fluid gel for use as a support bath in order to fabricate the tendon-on-chip constructs, the stock CNC colloidal suspension was first diluted to the desired concentration of 2.5 wt % and then a surface charge screening agent, i.e., calcium chloride (Sigma-Aldrich) at a concentration of 2.0×10^{-3} M, was added to induce the formation of a fluid gel.[23] Before the living structures were bioprinted, the colloidal fluid gel was sonicated for 1 min at 40% of the amplitude output for homogenization.

2.5. Cell Isolation and Culture. hASCs were obtained from lipoaspirate samples of the abdominal region of healthy donors undergoing plastic surgery under the scope of an established protocol with Hospital da Prelada (Porto, Portugal) and with the approval of the Hospital Ethics Committee (Approval No. 005/2019). The hASCs isolation procedure was performed following a previously optimized protocol.[40] hASCs were maintained in an α minimum essential medium (α-MEM; Sigma-Aldrich), supplemented with 10 vol % fetal bovine serum (FBS; Gibco, ThermoFisher Scientific) and 1 vol % antibiotic/antimycotic (A/A; Gibco, ThermoFisher Scientific) and incubated at 37 °C in a 5% CO_2 high-humidity environment, with medium replacements every 2−3 days. Cells until passage four were used for this study. Human umbilical vein cell line (EA.hy926; ATCC CRL-2922) was obtained from ATCC, LGC Standards, expanded, and cultured using Dulbecco's modified Eagle medium (DMEM)−low glucose (Sigma-Aldrich) with 10 vol % FBS (Gibco, ThermoFisher Scientific) and 1 vol % A/A (Gibco, ThermoFisher Scientific). All cultures were incubated at 37 °C in a 5% CO_2 high-humidity environment, with medium replacements every 2−3 days.

2.6. Preliminary Evaluation of the dECM Hydrogel Cytocompatibility by Live/Dead Assay. The cell viability was evaluated by a live/dead double-cell staining assay using Calcein AM and propidium iodide (PI). In a typical assay, hASCs (2×10^6 cells/mL) were mixed with neutralized dECM and 300 μL was poured into each well from a 48-well plate and cultured for 7 days. The viability was assessed at days 1 and 7 of culture to evaluate the cytocompatibility of the hydrogel. At each time point, the hydrogels were rinsed with PBS and incubated with Calcein AM [Invitrogen; 1:500 (v/v) in α-MEM for 30 min at 37 °C]. Samples were then rinsed with PBS and incubated in PI (Invitrogen; 1:1000 (v/v) in PBS for 15 min at 37 °C]. Finally, samples were washed with PBS and observed using a TCS SP8 confocal microscope (Leica Microsystems, Germany). Each experiment was performed in triplicate.

2.7. Preparation of Bioinks. Two bioink hydrogels were used for the development of the MPS: dECM for the tendon bioink and platelet lysate (PL) for the vascular bioink. To develop the tendon bioink, 1.0 and 2.0 wt % dECM were digested for 48 and 72 h, respectively, with 1 mg/mL pepsin in 0.02 M HCl, neutralized, mixed with hASCs (2×10^6 cells/mL), loaded into a sterile cartridge, and printed immediately. PL was produced from platelet concentrates obtained from healthy human blood donors, provided by "Serviço de Imunohemoterapia do Centro Hospitalar de S. João" (CHSJ, Porto, Portugal) under a previously established cooperation protocol and approved by the Hospital Ethical Committee (Approval No. 363/18). PL was produced according to a previously established protocol.[41] Briefly, the samples of platelet concentrates were pooled from 12 healthy human donors and subjected to three freeze−thaw cycles by freezing in liquid nitrogen, followed by heating at 37 °C in a water bath. The produced PL was aliquoted and stored at −80 °C until further use. These aliquots were then thawed at 37 °C for 5 min, centrifuged at 4000*g* for 5 min (centrifuge 5810R, Eppendorf, Germany), and then filtered with a 0.45 μm sterile filter (TPP, Switzerland). The endothelial cells (EA.hy926, 6×10^6 cells/mL) were then suspended in the resulting PL to produce the final vascular bioink.

2.8. Bioprinting of Tendon-on-CNC-Chip Models. A BioX bioprinter (Cellink, Sweden) with pneumatic printheads was used for the bioprinting experiments. Computer-aided designs (CADs) were created with the free online software *TINKERCAD* and saved as.stl (stereolithography) file format. Cartridges of 3 mL were loaded with bioinks and 25G blunt needles were used as nozzles. For printing of the monoculture systems, a pattern with dimensions of 13 × 13 mm (rectilinear pattern, without perimeter, 25% infill, 0.25 mm height) was designed. To print the tendon core constructs, the tendon bioink was placed in a temperature-controlled printhead that was used to maintain the temperature of the bioink between 4 and 11 °C and avoid its gelation inside the cartridge. To build the multicellular system, the tendon bioink was printed as described above, and the vascular bioink was printed as a square surrounding the tendon core compartment at a distance of 500 μm from this core structure and in the same *z* plane. The bioinks were directly printed within the support CNC fluid gel (2.5 wt % with 2.0×10^{-3} M Ca^{2+}) in 12-well plates prefilled with 1 mL of CNCs in each well. To ensure that the printed structures remained embedded within the CNC matrix and at a reachable *z* distance to allow confocal microscopy imaging of the cell-laden bioprinted hydrogels, all structures were printed 100 μm above the well surface. After printing, the CNC fluid gel was converted to a fibrillar matrix by adding an excess of a 7.5×10^{-3} M Ca^{2+} solution on top of the constructs, inducing the formation of stable hydrogels and locking the embedded bioprinted constructs. After 10 min, the Ca^{2+} solution was removed and changed by a cell culture medium.[23] Images depicting the successive steps of the chip fabrication process are shown in Figure S1. α-MEM with 10% FBS and 1% A/A was added to the monoculture systems, and 50:50 α-MEM/DMEM−low glucose with 10% FBS and 1% A/A was added to the multicellular systems. Finally, the samples were incubated at 37 °C in a 5% CO_2 high-humidity environment for up to 21 days, with medium replacement every 2−3 days. All formulations for each time point and assay were produced in quadruplicate.

2.9. Analysis of the Chip Microstructure by High-Resolution Field-Emission Scanning Electron Microscopy (SEM). The microstructure of the dECM hydrogel embedded within a CNC support chip was accessed by high-resolution SEM (Auriga Compact, Zeiss). Before SEM analysis, 2.0 wt % dECM ink was printed and locked within the CNC fibrillar matrix. After locking, the samples were washed with water and solvent-exchanged with ethanol (Thermo Fisher) solutions of increasing concentrations (5%, 15%, 25%, 40%, 70%, 90%, and 100% v/v) for 4 h each step. After solvent exchange, ethanol was removed by critical point drying (Autosamdri-815 Series-A, Tousimis) with liquefied CO_2. To expose the dECM microstructure embedded within the CNCs, the samples were freeze-fractured after immersion in liquid nitrogen and then sputter-coated with 1 nm of platinum (EM ACE600 Leica). Samples were observed by SEM with an accelerating voltage of 3 kV.

2.10. Cell Viability, Morphology, and Immunocytochemistry of the Developed MPS. The impact of the printing process on the cell viability was assessed at days 1 and 11 of culture after printing on the monoculture systems by live/dead assay. At each time point, the printed chip samples were rinsed with PBS and incubated with Calcein AM [Invitrogen; 1:500 (v/v) in α-MEM for 45 min at 37 °C]. Samples were rinsed with PBS and then incubated in PI [Invitrogen; 1:200 (v/v) in PBS for 30 min at 37 °C]. Finally, the samples were washed with PBS and observed using a TCS SP8 confocal microscope (Leica Microsystems, Germany). Each experiment was performed in triplicate. For immunolabeling procedures on chip, monoculture and multicellular samples after 21 days of culture were washed with PBS and fixed with 10% (v/v) neutral buffered formalin at RT. After fixing, samples were washed thoroughly with PBS and kept at 4 °C in PBS until further use. For histological processing, after formalin fixation, the samples were embedded in paraffin for further sectioning using a microtome (HM355S, Microm,

https://doi.org/10.1021/acsami.2c22371
ACS Appl. Mater. Interfaces 2023, 15, 50598−50611

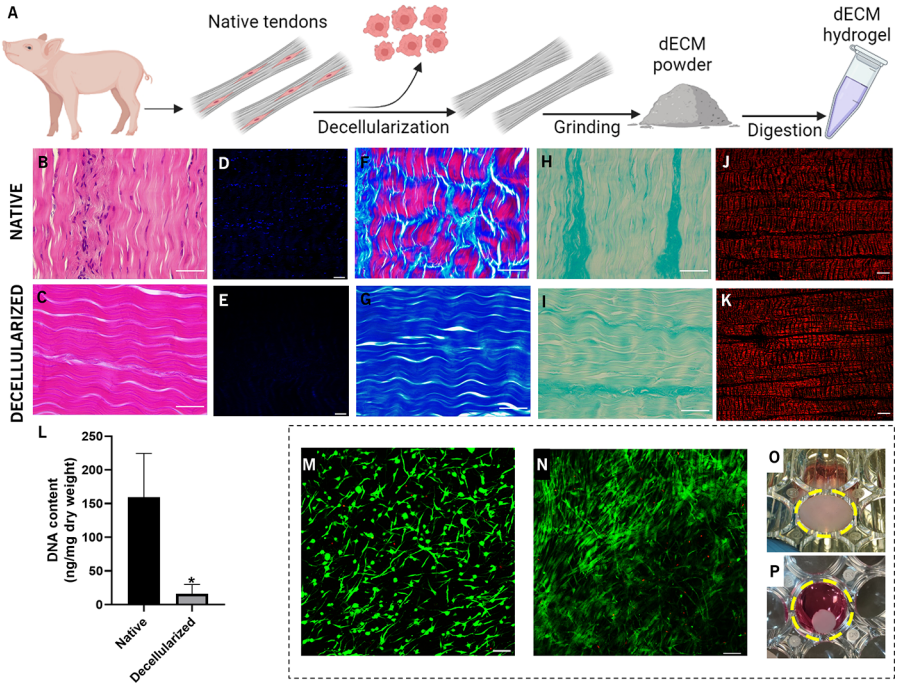

Figure 2. Tendon dECM development. (A) Schematic representation of the dECM hydrogel solution preparation. The process starts with the harvesting and dissection of porcine tendons, followed by decellularization, grinding, and digestion of the dECM powder, resulting in a homogeneous hydrogel precursor solution. (B–L) Removal of genetic material and preservation of the tendon ECM after decellularization: histological sections of native (B, D, F, H, and J) and decellularized (C, E, G, I, and K) tendons stained with H&E (B and C; nucleus in purple) and DAPI (D and E; nucleus in blue), MT staining (F and G) for collagenous structure (blue) and cytoplasmic components (red), AB staining (H and I) for GAG and PSR staining (J and K) for Col-I (red) and Col-III (green) under polarized light; DNA quantification (L) was assessed after decellularization, and native tissues were used as the control. (M–P) Preliminary evaluation of the dECM hydrogel cytocompatibility by live/dead assay at days 1 (M) and 7 (N) of culture (green, live cells; red, dead cells) and respective images depicting their volume contraction from day 1 (O) to day 7 (P) of culture. Scale bars: (B–I) 50 μm; (J and K) 200 μm; (M and N) 100 μm. Values are plotted as the mean ± standard deviation. *, $p < 0.05$ ($n = 3$).

Thermo Scientific), obtaining histological sections of 20 μm thickness. The histological sections were then deparaffinized, and a heat-induced epitope retrieval technique was used for antigen retrieval. Briefly, a solution of citrate buffer (pH = 6.0) was heated in a microwave for 2 min. Then, slides were placed inside the buffer and heated for 4 min. Thereafter, the slides were allowed to cool at RT for 30 min and then washed three times with deionized water. After this point, both chip and histological sections were permeabilized with 0.2% (v/v) Triton X-100 in PBS for 30 min and then blocked with 3% (w/v) bovine albumin serum (BSA) in PBS for 1 h at RT. Thereafter, monoculture and multicellular chips/sections were incubated overnight at 4 °C with a primary antibody against tenomodulin (TNMD; rabbit anti-TNMD antibody, 1:100, Abcam ab203676), scleraxis (SCX; rabbit anti-SCX antibody, 1:200, Abcam ab58655), type I collagen (Col-I) (rabbit anti-collagen I antibody, 1:100, Abcam ab34710), or type III collagen (Col-III) (rabbit anti-collagen III antibody, 1:100, Abcam ab7778), diluted in a solution of 0.2% (v/v) Triton X-100 in PBS with 1% BSA (w/v). Multicellular chips/sections were incubated with the antibody CD31 (APC-conjugated mouse antihuman CD31/PECAM-1 monoclonal antibody, R&D Systems, FAB3567A), diluted in a solution of 0.2% (v/v) Triton X-100 in PBS with 1% BSA (w/v), overnight at 4 °C while protected from light. Immunolabeled chips/sections were then washed with PBS three times for 15 min and incubated with the corresponding secondary antibody labeled with Alexa Fluor 488 [donkey antirabbit IgG (H+L), A21206, ThermoFisher Scientific, 1:200] for 3 h at RT while protected from light. After washing with PBS, the nuclei and cytoskeleton of all samples were stained with DAPI (1:1000 in PBS) and phalloidin-TRITC (1:200 in PBS), respectively, for 1 h at RT. All of the steps for the sample preparation were performed under gentle agitation in an orbital shaker. After washing, the samples were kept in PBS and the histological sections were mounted with a Vectashield fluorescence mounting medium (Vector Laboratories) and analyzed using a TCS SP8 confocal laser scanning microscope (Leica Microsystems, Germany). Each experiment was performed in triplicate. The directionality of the cell cytoskeleton in the maturated constructs was evaluated using *ImageJ* software, with the "Directionality" plugin, by a Fourier components method, with Nbins equal to 180, as described in our previous study.[23]

2.11. Gene Expression. The expressions of TNMD, SCX, tenascin C (TNC), Col-I, Col-III, and vascular endothelial growth factor A (VEGF-A) genes were determined by real-time polymerase chain reaction (RT-PCR) analysis. The samples were washed twice with PBS and crushed into Eppendorfs, and the total RNA was extracted with a reagent (TRIzol Reagent, Thermo Fisher Scientific), according to the manufacturer's instructions. The extracted RNA was analyzed with a NanoDrop ND-100 spectrophotometer (Thermo-Scientific). A qScript cDNA SuperMix kit (Thermo Fisher Scientific) was used for the reverse transcription to cDNA. The quantitative polymerase chain reaction was carried out for quantification of the transcripts using the PerfeCTA SYBR Green FastMix kit following the manufacturer's protocol, in a Real-Time Mastercycler Realplex thermocycler (Eppendorf, Germany). The primers (Table S1) were predesigned with *PerlPrimer*, version 1.1.21, software and synthesized by MWG Biotech. Glyceraldehyde 3-phosphate dehydrogenase (GAPDH) was used as the housekeeping gene. The ΔΔCt method was selected to evaluate the relative expression level for each target gene. All gene expression values were normalized against the expression levels of GAPDH used as the reference gene. In the case of a monoculture model, the relative expression of target genes was related to its respective expression levels at day 1. For the multicellular experiments, the relative expression of the tenogenic gene was related to its respective expression levels in the monoculture model, while the

https://doi.org/10.1021/acsami.2c22371
ACS Appl. Mater. Interfaces 2023, 15, 50598–50611

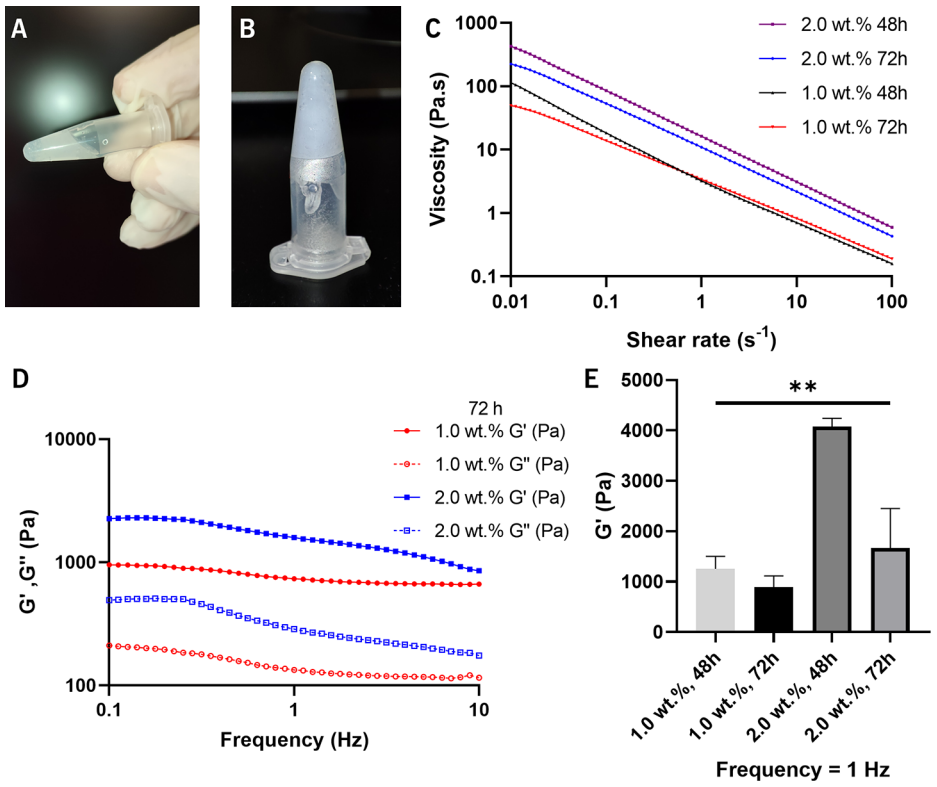

Figure 3. Characterization of a tendon dECM solution. Representation of the dECM solution (A) before and (B) after gelation, forming a consistent hydrogel. (C) Shear viscosity of 1.0 and 2.0 wt % dECM, digested for 48 and 72 h, at 4 °C. (D) Frequency-dependent oscillatory shear rheology of 1.0 and 2.0 wt % dECM digested for 72 h and incubated at 37 °C (G', storage modulus; G'', loss modulus). (E) Storage modulus (G') of 1.0 and 2.0 wt % dECM digested for 48 and 72 h and incubated at 37 °C at 1 Hz of frequency. The 2.0 wt % dECM digested for 48 h is significantly different from all of the other groups, with ** representing the statistical significance for $p < 0.01$ ($n = 3$).

VEGF-A expression was normalized to the levels of day 1 because its expression in monoculture (control group) was below the detection limits of the assay ($n = 3$, independent experiments).

2.12. Statistical Analysis. All experimental data are expressed as mean ± standard deviation. For statistical analysis, the two-tailed Student's t test was used for the comparison of two groups, while one-way analysis of variance was applied for a comparison between three or more groups. Statistical analysis was performed using *GraphPad Prism*, version 8.0 (GraphPad Software Inc.). The significance for all statistical analyses was defined as $p < 0.05$. All of the experiments were performed in triplicate unless otherwise stated.

3. RESULTS AND DISCUSSION

3.1. Porcine Tendon Decellularization. The preparation of dECM hydrogel solutions is a process involving multiple steps (Figure 2A), which starts by harvesting and dissecting porcine tendons, followed by decellularization. To access the efficiency of the decellularization process, the cellular content and retention of ECM structural components were evaluated in both native and decellularized tendon tissues. Typically, decellularization criteria consider an effective tissue decellularization for a DNA content of <50 ng of dsDNA per mg of dECM and demonstrate the absence of a nuclear material in the dECM by histological or other cell staining analysis.[42−44] As can be observed by H&E and DAPI staining, in the native tissue (Figure 2B,D) cells are shown to be aligned between the crimp patterns of the collagenous ECM, being more densely packed between the fascicles in the endotenon regions. After decellularization, these stainings demonstrate the absence of nuclei in the matrix (Figure 2C,E). Moreover, MT staining also demonstrates the complete removal of cytoplasmic residues (red) while preserving most of the collagenous structure (blue) (Figure 2F,G). Similarly, despite some loss of GAGs, other acidic glycoproteins can be noticed after decellularization compared to the native tissue, and AB staining (Figure 2H,I) shows good preservation of these components in the dECM. As expected, SRP staining shows that the fibrillar and crimped Col-I (red) is the prevalent collagen type identified in both samples (Figure 2J,K). The results obtained by H&E and DAPI imaging were corroborated by DNA quantification (Figure 2L), where the residual DNA content detected in the dECM was 16.1 ± 13.7 ng/mg, lower than the established limit of 50 ng/mg of dECM.[42−44] Overall, the decellularization process was revealed to be effective in removing the cellular content while preserving the general biochemical and structural signature of the native ECM.

To exclude potential cytotoxic effects of the dECM derived due to the presence of remanent detergents or enzymes from the decellularization process,[45] the cytocompatibility of the developed dECM hydrogel was preliminarily evaluated before the bioprinting steps. hASCs were mixed with dECM hydrogels (2.0 wt %) and tested by live/dead assay at days 1 (Figure 2M) and 7 (Figure 2N) of culture. Overall, encapsulated cells in the hydrogels show good viability and proliferation over time. Macroscopically, the hydrogel suffers a significant volume contraction along the culture time (Figure 2O,P), suggesting the ability of cells to attach and remodel the hydrogel, reshaping the surrounding matrix environment, an effect that is in accordance with previous studies on dECM hydrogels.[31,45,46]

https://doi.org/10.1021/acsami.2c22371
ACS Appl. Mater. Interfaces 2023, 15, 50598−50611

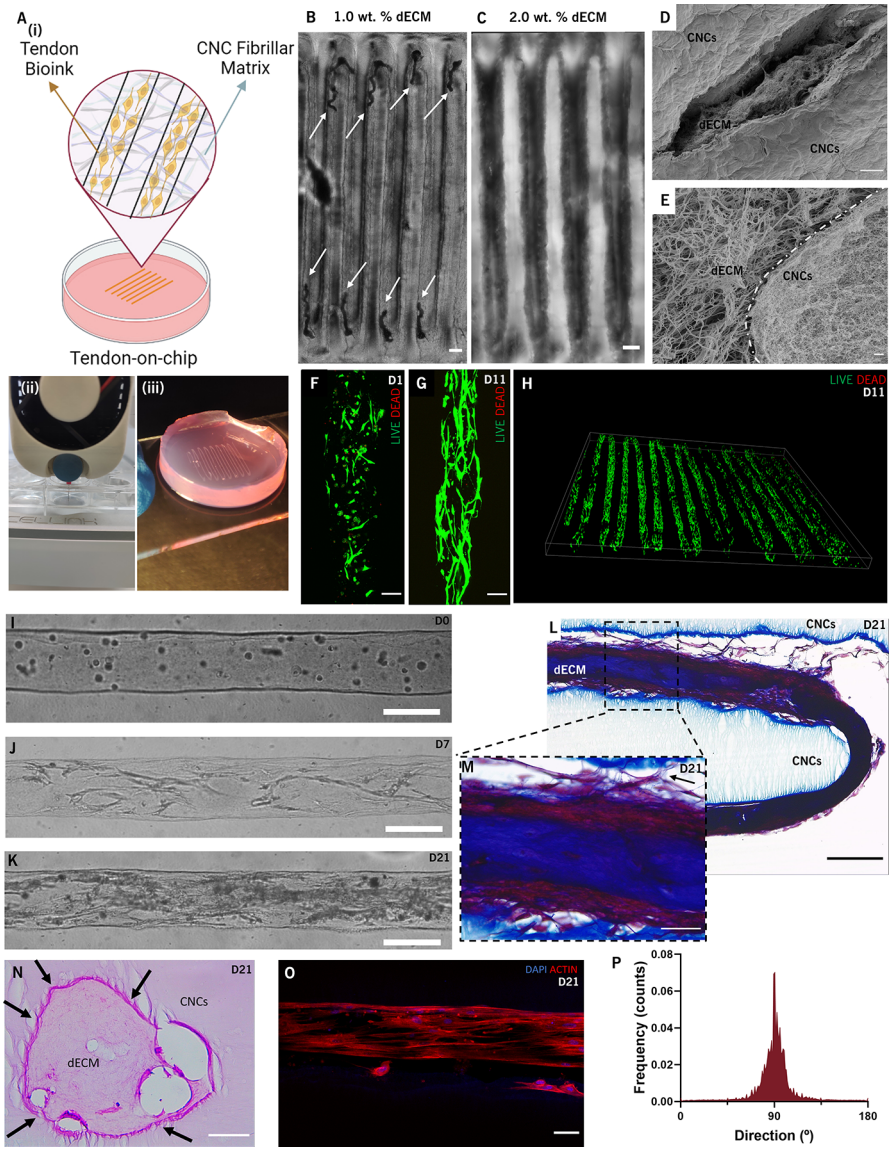

Figure 4. Development of the monoculture tendon-on-chip model. (A) (i) Schematic representation of the monoculture system design, (ii) photograph of the printing step within the CNC fluid gel, and (iii) photograph of the resulting monoculture system locked within the CNC chip. Bright-field confocal laser microscopy (CLM) images of (B) 1.0 wt % dECM bioink after 7 days of culture showing contraction and retraction of the hydrogel filaments (arrows) and (C) 2.0 wt % dECM bioink showing no contraction after 7 days of culture. SEM images of (D) the dECM hydrogel embedded within the CNCs fibrillar matrix and (E) the interface between dECM (left) and the CNCs fibrillar matrix (right). Evaluation of the embedded cell viability by live/dead staining at days 1 (F) and 11 (G) of culture, with the 3D reconstruction of the full tile of the system (H) (green, live cells; red, dead cells). Transmitted light microscopy images of the cell morphology and density at days 0 (I), 7 (J), and 21 (K) of culture. (L and M) MT staining of the longitudinal histological section of the monoculture construct after 21 days of culture. (N) H&E staining of the histological cross section of the monoculture system after 21 days of culture. (O) CLM image of cellular cytoskeleton organization after 21 days of culture and (P) the respective directionality analysis. Scale bar: (B and C) 1 mm; (D and M–O) 50 μm; (E) 1 μm; (F and G) 100 μm; (I–L) 200 μm.

3.2. Development and Characterization of the dECM Ink. The general protocol of dECM hydrogel production involves enzymatic digestion of the dECM powder, neutralization (Figure 3A), and gelation of the hydrogel after incubation at 37 °C (Figure 3B). After digestion, the dECM gelation ability was confirmed by visual inspection, observing a solution color change from clear to cloudy, as well as by an inversion test, confirming the formation of a nonflowing semisolid hydrogel at the bottom of the flask.

The rheological properties of hydrogel bioinks are key parameters to access their printability in extrusion-based 3D bioprinting systems.[47] Thus, the rheological behavior of dECM hydrogels at two different concentrations (1.0 and 2.0 wt %) and digestion times (48 and 72 h) was characterized. Shear viscosity measurements of precursor dECM solutions (Figure 3C) showed that all formulations exhibit a clear shear-thinning behavior at 4 °C, a characteristic that is known to favor cell viability in extrusion bioprinting applications.[47] Higher dECM concentration results in solutions with increased zero-shear rate viscosity, while an increase of the digestion time leads to less viscous solutions.

dECM-based hydrogels have abundant collagenous proteins that facilitate their self-assembly into cross-linked networks under physiological pH and temperature conditions, which is a

https://doi.org/10.1021/acsami.2c22371
ACS Appl. Mater. Interfaces 2023, 15, 50598–50611

particular advantage of these systems.[32,48] Frequency-dependent oscillatory testing showed the typical solidlike behavior of these types of dECM hydrogels, independent of their concentration [storage modulus (G') higher than the loss modulus (G''); Figure 3D], indicating their ability to retain their shape after printing.[31−33] On the other hand, while increasing dECM concentration results in hydrogels with higher storage modulus, an increase in the digestion time logically decreases the storage modulus (Figure 3E). These results are in good agreement with previous studies on tendon dECM bioinks, which compared different digestion times and hydrogel concentrations to achieve the best formulations for bioprinting.[31,33,37]

3.3. Fabrication and Characterization of the Tendon-on-CNC-Chip. After characterization of the hydrogel formulation, the MPSs were then developed. Here, we aimed at developing two different MPSs: a monoculture system intended to recreate the physiological characteristics of a healthy tendon core microenvironment and a multicellular system to study the crosstalk between the tendon stroma and cells from the extrinsic compartment, namely, vascular cells.

The first step to fabricate the tendon core system (Figure 4A) was to test and select the ink formulation that would be more appropriate to enable the proposed concept. In extrusion bioprinting processes, the higher the viscosity of the bioink, the higher the pressures required to extrude it, potentially leading to increased shear stresses, which can negatively affect the cell viability.[47] Thus, a compromise between the dECM concentration and digestion time needs to be established in order to allow printing processes without exerting excessive cell stress, while simultaneously providing a proper cell niche to sustain cell growth and proliferation. Based on the rheological characterization of the inks, the 2.0 wt % dECM digested for 48 h was judged to be too viscus to be extruded without harming the cells, while the 1.0 wt % dECM digested for 72 h resulted in soft hydrogels with very low mechanical integrity. These two formulations were therefore excluded from further testing. For a first assessment on the structural integrity of bioprinted structures, hASCs were suspended in the two selected dECM inks, printed within the CNCs fluid gel and then locked into the CNC fibrillar matrix, where they were maintained in culture for 7 days. This simple locking step is achieved by adding a Ca^{2+} solution on top of the embedded construct,[23] inducing the self-assembly of a CNC fluid gel into a stable fibrillar matrix that acts as a stable tailor-made support bioreactor for long-term maintenance and maturation of printed living structures. Because heathy adult tendons are low vascularized tissues where tenocytes reside embedded within a dense collagen fiber matrix under lower oxygen levels compared to other vascular-rich organs and tissues,[49] here we opted for not including perfusable channels. Although there is no microfluidic flow in this system, according to a recent board definition,[50,51] we believe it can be considered an organ-on-a-chip device because the platform has a significant engineering component and spatial cell compartmentalization. However, as we have previously demonstrated, this CNC-based platform supports the direct print of perfusable channels using, e.g., fugitive inks, allowing the complexity of the proposed chip design to evolve, if needed. As shown in Figure 4B, 1.0 wt % dECM bioink filaments broke and retracted to the corners of the construct, demonstrating that this low dECM concentration was unable to support the contractile forces resulting from cell attachment, proliferation, and remodeling activity while maintaining the shape fidelity of the printed structures. In contrast, the structures printed with the 2.0 wt % dECM bioink showed no contraction or retraction, maintaining its shape during the culture time (Figure 4C). To assess the chip microstructure and evaluate whether dECM was able to fibrillate within the CNC support matrix, the acellular dECM ink was printed and locked in this material following the same conditions of the cellular constructs. Their cross sections were then analyzed by SEM after critical point drying and cryogenic fracturing. The exposed cross section of the chip (Figure 4D) shows a hierarchical fibrous arrangement, with the fibrillated dECM embedded and compartmentalized within a nanoscale CNC fibrillar network, mimicking the structural features of basement membranes and parenchyma ECMs.[23] The interface between these two materials (Figure 4E) shows some physical entanglement that occurs during the simultaneous gelation of dECM and the self-assembly of CNCs.

The images of live/dead assay show that cells in this monoculture system have high viability after the printing process (Figure 4F) and during culture up to 11 days (Figure 4G,H). To confirm the ability of this system to support cell growth and proliferation, it was cultured for 21 days. Because the CNC matrix is transparent, it allows optical monitoring of the samples throughout the time of culture. At day 0 (Figure 4I), the printed cells look homogeneously distributed throughout the bioink filaments. After 7 days of culture (Figure 4J), the cells started to stretch, showing elongated morphology, and established cell-to-cell contacts. At the end of 21 days of culture (Figure 4K), the printed patterns are densely filled with cells, nicely stretched, and aligned along the filament direction without visible contraction of the dECM bioink within the CNCs, in contrast with what happens when these dECM hydrogels are directly cultured on well-plates (Figure 2P) or when a lower concentration of dECM is applied in the system (Figure 4B). This marked cell elongation and alignment along the filament direction shows that the synergy between the dECM cues and printed patterns is able to induce anisotropic cell organization resembling tenocyte morphology in tendon tissues.[32,37]

Next, we aimed to demonstrate the processing versatility of the proposed tendon-on-CNC-chip platform in cell biology characterization workflows. Standard staining and immunohistochemistry labeling can be directly performed and analyzed by microscopy techniques on chip, without disturbing the printed constructs. However, these systems can also undergo typical histological sectioning protocols without requiring the previous release of the cultured structures, which is an advantage over the general organ/tissue-on-chip housed on plastic microfluidic devices.[23] To demonstrate this potential and assess the collagenous structure and ECM organization of the cultured tendon core, histological sections of the tendon-on-CNC-chip (cultured for 21 days) were stained with MT (Figure 4L,M) and H&E (Figure 4N). Interestingly, a recent study has compared the behavior of cells seeded in high-density collagen gels when unclamped or clamped to provide uniaxial tension.[46] As expected, unclamped gels suffered significant volume contraction and showed unorganized structure, while clamped constructs developed hierarchical collagen organizations, similar to native juvenile tendon tissue.[46] Similarly, our dECM hydrogel also suffers significant contraction with unorganized cells in the dECM hydrogels cultured in well-plates (Figure 2N,P), while when printed and cultured within the CNC support matrix, the constructs reorganize into dense

https://doi.org/10.1021/acsami.2c22371
ACS Appl. Mater. Interfaces 2023, 15, 50598−50611

collagen (blue) filaments showing high cell density (red) (Figure 4L,M). In these systems, the results suggest that the fixed paths in the CNC matrix act as "anchors" that contribute to maintenance of the bioink under tension during culture, allowing densification of the dECM structure (Figure 4L,M). MT staining also shows that the cells and collagenous structures establish a close connection with the CNC fibrillar material (arrow in Figure 4M), while H&E staining of cross sections of embedded filaments (Figure 4N) confirms that the dECM hydrogel does not undergo extensive volume contraction, remaining entangled with the CNC network (arrows) and demonstrating interfacial integration between the two materials. It should be noticed that the apparent filament contraction seen in Figure 4L,N is most likely derived from the hydration, dehydration, and sectioning steps during the sample preparation for histological analysis. Nevertheless, the possibility that these dECM contraction effects result from cell activity during the time of culture cannot be completely excluded and should therefore be further evaluated in detail in future studies. On the other hand, the high uniaxial alignment and elongated cell morphology was also confirmed by directionality analysis of the cell cytoskeleton in the maturated constructs (Figure 4O,P), suggesting the adoption of a tenocyte-like morphology. Thus, by preserving the spatial organization of the printed patterns during *in vitro* maturation of the constructs, this system additionally contributes to induction of the characteristic uniaxial cell alignment of tendon tissues, which is a significant challenge to achieve within hydrogel biomaterials. Interestingly, the mechanosignaling resulting from the maintenance of cellular tension, similar to that recreated in our systems, has recently been shown to be essential in regulating the mechanism through which tendon cells preserve their homeostasis.[52]

Due to the previously discussed limitation of primary human tenocytes as cell sources for *in vitro* modeling,[34,53] here we have used the widely available and easy to obtain hASCs, which can be stimulated to differentiate into the tenogenic phenotypes.[35,54,55] Following the strategy of previous studies,[31−33,56] our hypothesis was that the biophysical and biochemical cues of the tendon dECM would synergistically guide hASCs differentiation toward the tenogenic lineage without requiring additional supplementation with biological factors. To assess the tenogenic commitment of hASCs in our MPS, both gene expression and immunolabeling analysis were performed. Gene expression analysis (Figure 5A) shows a significant increase in the expression of SCX and TNMD, two of the mostly recognized tendon-related markers.[4,57] TNMD is known to be positively regulated by the transcription factor SCX in a tendon-cell-lineage-dependent manner.[58] Here, an increase on the expression of SCX is also followed by a significant increase of TNMD. While variation of the Col-III expression is not significant during the culture time, Col-I, which is the predominant collagen type in mature tendons,[2] increases significantly. The expression of these tendon phenotypes (SCX and TNMD) and matrix (Col-I and Col-III)-related protein[54,59] was further confirmed by immunofluorescence analysis in both the CNC-embedded constructs and their histological sections. As expected, embedded cells show a time-dependent expression of both tenogenic markers, which increase over the time of culture (Figure 5B−G), and the *de novo* secretion of tendon matrix proteins (Figure 5H,I). Taken together, these results demonstrate that the synergistic effects of the tendon dECM and construct architecture can

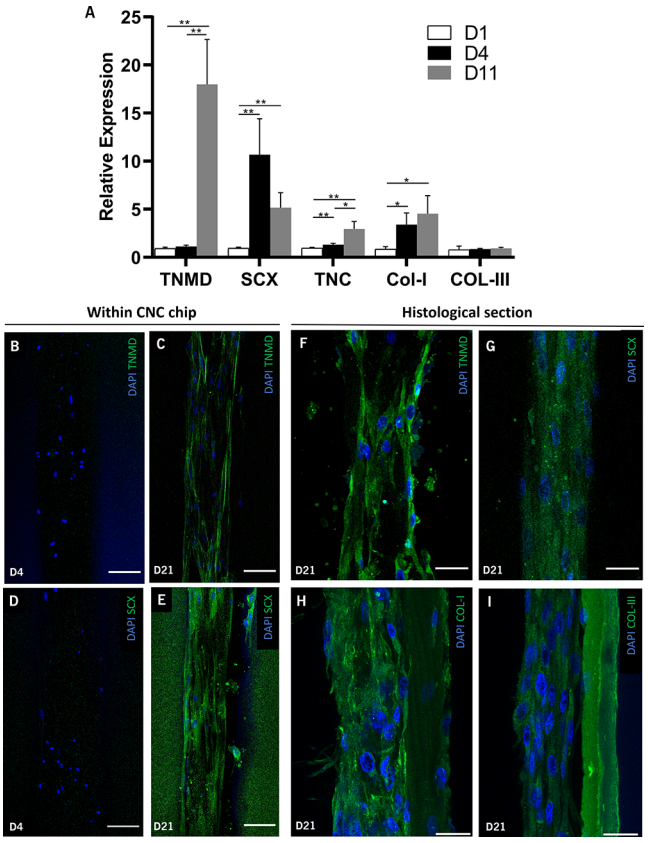

Figure 5. Evaluation of the monoculture system phenotypes. (A) Gene expression profile of tendon-related markers. The relative expression data are normalized to the gene expression levels at day 1. Confocal fluorescence images of TNMD at days 4 (B) and 21 (C and F), SCX at days 4 (D) and 21 (E and G), and Col-I (H) and Col-III (I) cultured for 21 days, directly stained on the chip (B−E) or on histological sections (F−I). Scale bar: (B−E) 75 μm; (F−I) 25 μm. Statistical significance: *, $p \leq 0.1$; **, $p \leq 0.01$; ***, $p \leq 0.001$; ****, $p \leq 0.0001$ ($n = 3$).

successfully induce the commitment of hASCs toward the tenogenic lineage. Overall, the proposed system combines the advantages of 3D free-form bioprinting using mechanically weak but tenoinductive dECM-based bioinks with the structural support provided by CNC housing devices for allowing the automated on-plate arraying of multiple independent 3D tendon models, as well as for their long-term maintenance and maturation. Additionally, all of these advantageous features are achieved while maintaining compatibility with external analysis platforms and microscopy imaging modalities.

3.4. Tendon Core−Vascular Cells Crosstalk on the Tendon-on-CNC-Chip. Healthy mature tendons are hypovascular tissues in which blood vessels are mainly present in the endo and epitenon. Nevertheless, it still depends on the vascular network for the delivery of cells, GFs, cytokines, nutrients, and oxygen needed for function.[53] One hallmark of tendinopathy and healing tendons is the increased vascularization and scar tissue formation.[4] On the other hand, tissue vascularization and cellularization are also increased at the tendon development stages.[60] The exact crosstalk mechanisms existing between the vascular and tendon core cells are, however, poorly understood.[61] Thus, vascular cell populations should be considered and studied when developing physio-

https://doi.org/10.1021/acsami.2c22371
ACS Appl. Mater. Interfaces 2023, 15, 50598−50611

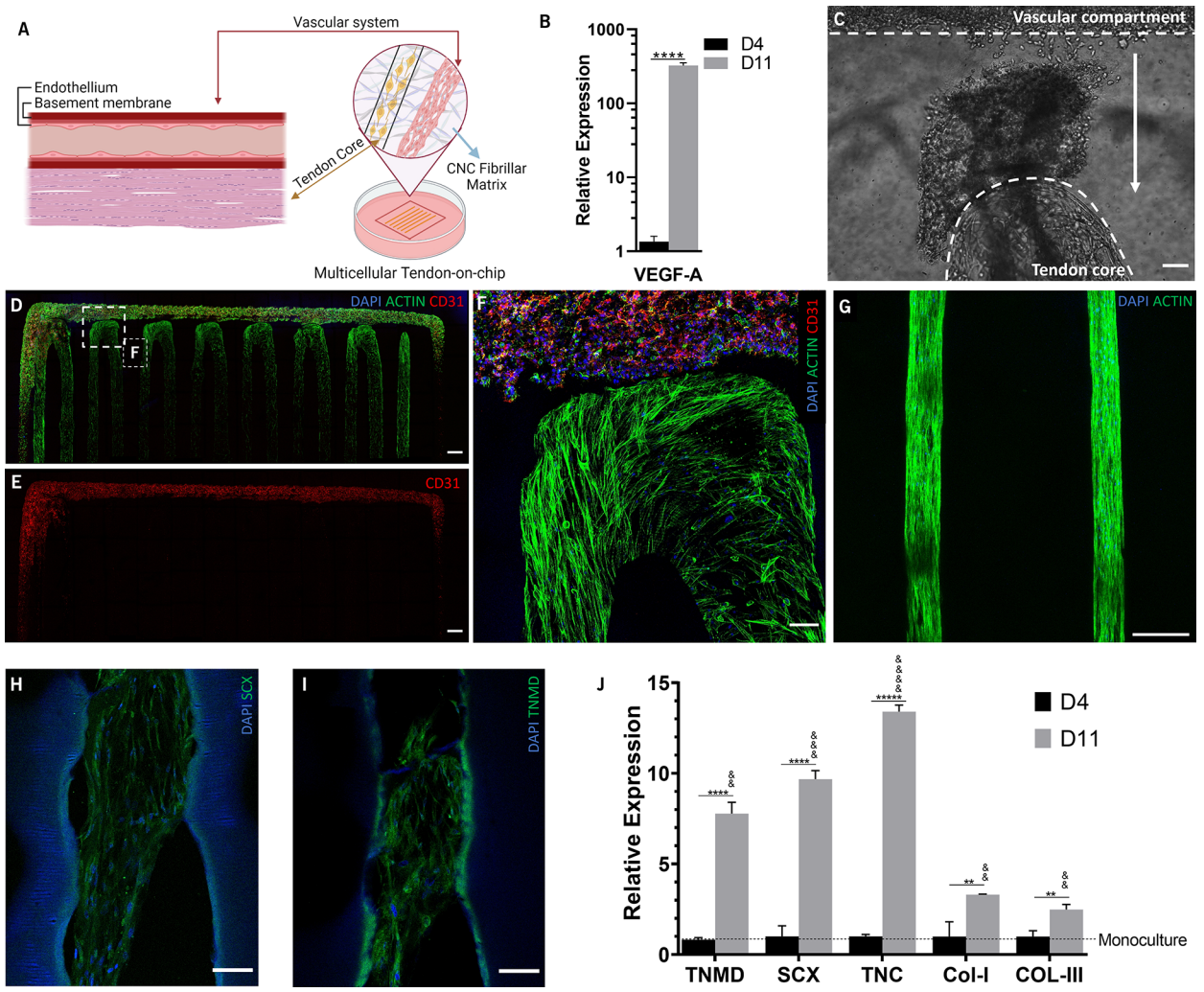

Figure 6. *In vitro* evaluation of the multicellular tendon-on-CNC-chip. Schematic representation of the multicellular construct design (A). Gene expression of VEGF-A in cells of the tendon core of the multicellular systems (B). Transmitted light microscopy images of endothelial cells migrating toward the tendon compartment at day 11 of culture (C). CLM image of the multicellular construct (D), with a focus on the endothelial cells spatial distribution (E) in the system at day 21 of culture. CLM image of the interface between the vascular and tendon core compartments (F). CLM image of the tendon core compartment at day 21 (G). Evaluation of the tenogenic differentiation of hASCs after 21 days of culture by immunolabeling of SCX (H) and TNMD (I) in the histological section. Scale bar: (D and E) 1 mm; (C and F) 100 μm; (G) 250 μm; (H and I) 75 μm. Gene expression of the tenogenic (J) markers in the tendon core cells of the multicellular systems. The relative expression of tenogenic genes are normalized to the gene expression levels of the monoculture system (J), and the VEGF-A expression is normalized to the gene expression levels at day 1 (B). & indicates statistical significance relative to monoculture system. * indicates statistical significance relative to the time of culture. Statistical significance: *, $p \leq 0.1$; **, $p \leq 0.01$; ***, $p \leq 0.001$; ****, $p \leq 0.0001$; &, $p \leq 0.1$; &&, $p \leq 0.01$; &&&, $p \leq 0.001$; &&&&, $p \leq 0.0001$ ($n = 3$).

logically relevant *in vitro* models of tendon health and disease.[53]

Having demonstrated the ability to fabricate the tendon stromal compartment, we next used an endothelial cell bioink to build multicellular MPSs and study their crosstalk with the tendon core in a biomimetic compartmentalized construct (Figure 6A). Here, the vascular bioink consisted of endothelial cells suspended in human PL, a human blood derivative that has been widely used as a cell culture supplement and a bioactive scaffolding biomaterial in tissue engineering strategies.[62−64] As a biomaterial, PL is a low-viscosity solution that exhibits near-Newtonian liquid behavior and results in a very soft hydrogel with typical storage modulus below ∼20 Pa (Figure S2).[41,64] PL-based hydrogels have shown superior performance as matrices for endothelial cell growth and maintenance of their cellular characteristics compared to other alternatives such as fibrin or collagen hydrogels,[65,66] properties that we have previously explored to formulate a bioink for endothelial cells printing.[23] Unexpectedly, during the time of culture, endothelial cells started to migrate toward the direction of the tendon compartment (Movies S1 and S2), showing the existence of chemoattraction between these two systems, as well as the ability of endothelial cells to physically remodel the CNC network. The existence of this signaling among cells was further evaluated by analysis of the gene expression of VEGF-A on the differentiation of hASCs, which is a potent angiogenic factor that regulates blood vessel formation in tendon development and healing.[67] While in the monoculture system the VEGF-A expression is below the detection limit of the assay, in the multicellular system, it is significantly increased after 11 days of culture (Figure 6B). These results suggest that soluble biochemical factors secreted

https://doi.org/10.1021/acsami.2c22371
ACS Appl. Mater. Interfaces 2023, 15, 50598−50611

by endothelial cells trigger VEGF signaling on the tendon core cells. However, endothelial cells seem to accumulate at the interface of tendon compartment filaments (Figure 6C). To better understand the behavior and positioning of the endothelial cells, these multicellular systems were stained for CD31 (red) as an endothelial marker, while F-actin (green) was stained to visualize the cytoskeleton of the whole cells in the system. Confocal fluorescence microscopy images showed that, although endothelial cells migrate toward the tendon compartment, their infiltration within this structure is not significant (Figure 6D,E), tending to accumulate at the interface of the filaments instead of invading it (Figure 6 F). On the other hand, the tendon compartment is filled with hASCs, nicely stretched and aligned along the construct filaments (Figure 6 G).

To evaluate the potential effects stemming from this cellular crosstalk on the tenogenic commitment of hASCs, changes on the gene expression profile of the tendon core compared to the monoculture system were assessed and histological sections of the multicellular MPS were immunolabeled for tenogenic markers. Similar to that observed in monoculture constructs, immunolabeled cells of the tendon compartment also express SCX (Figure 6H) and TNMD (Figure 6I) proteins after 21 days of culture. Moreover, the gene expression results demonstrated that its tenogenic markers (Figure 6J) were in general significantly upregulated compared to the monoculture system. Besides the two tenogenic markers SCX and TNMD, the main tendon matrix-related genes were also upregulated, namely, Col-I and Col-III and the glycoprotein TNC.[4] Interestingly, although existing data on these tendon cell interactions are scarce, VEGF was shown to inhibit the undesired adipogenic differentiation of tendon stem/progenitor cells[68] and similar pro-tenogenic effects have been previously reported when tenocytes were cocultured with HUVECs on fibrous scaffolds.[69] On the other hand, the presence of molecular components with known antiangiogenic properties, such as TNMD,[70] either secreted by differentiating hASCs or due to its remnant presence in the tendon dECM, might justify why endothelial cells tend to accumulate at the interface with the tendon core (Figure 6F) instead of infiltrating within these structures. Nevertheless, the possibility that endothelial cells might also be deterred by physical constraints related with an increased dECM densification occurring during culture is a hypothesis that cannot be completely excluded.

Altogether, these results show that endothelial cells establish a compartmentalized biochemical crosstalk with the tendon core constructs that favors their tenogenesis and maturation. Accordingly, this MPS seems to be recreating the characteristic microenvironment of tendon development. It is worth noting that while in this study we focused on establishing the key fabrication principles and basic functional assessment of the proposed MPS for providing a proof-of-concept, in-deeper screening of the biological crosstalk occurring in this system by applied, e.g., advanced transcriptomic and proteomic tools, will allow further elucidation of the key cellular and molecular pathways taking place in this model. How it will evolve for longer maturation periods, more specifically, if it will progress toward a homeostasis state or degenerate toward a more disease like situation, is an interesting research subject that should be further investigated in follow-up studies in order to elucidate its detailed mechanisms.

In summary, the mono- and multicellular systems developed in this work can be useful tools not only for the cellular and molecular characterization of tendon physiology and pathological mechanisms but also for a study of the therapeutic effect of new drugs, while reducing preclinical tests in animal models. It would be particularly interesting, for example, to study the mode of action of innovative RNA-based therapies, which are currently entering early-stage clinical trials.[7,71,72]

4. CONCLUSIONS

In this work, we were able to successfully develop two humanized tendon-on-CNC-chip systems with increasing complexity by combining the principles of matrix-assisted bioprinting and nanomaterial self-assembly. We first produced a tendon dECM-based bioink suitable for bioprinting. Then, we developed a 3D monoculture system embedded within its own fibrillar support matrix that is capable of sustaining compartmentalized *in vitro* cell culture and guiding hASCs toward tenogenesis. This system was next used to study the interaction between the tendon core tissue and cells of the vascular system. Remarkably, endothelial cells migrated toward the tendon compartment without infiltrating it, suggesting the recreation *in vitro* of the antiangiogenic effect that occurs in healthy mature tendon stroma. Remarkably, the presence of endothelial cells was shown to significantly boost the tenogenic commitment of hASCs.

Overall, the results demonstrate that our humanized tendon-on-CNC-chip can recapitulate some key features of the developing tendons' microenvironment. The automated biofabrication platform established here further opens the possibility of easily adapting or increasing the complexity of the system by, for example, incorporating other relevant tendon cell populations of interest and perfusable channels for dynamic culture. This humanized *in vitro* MPS represents thus an interesting tool for studying tendon physiology and the underlying mechanism of tendon diseases. Ultimately, these models can be useful for testing new drugs for the treatment of tendinopathy, contributing to the increased efficiency of drug discovery pipelines and reduction of preclinical animal experimentation.

■ ASSOCIATED CONTENT

Supporting Information

The Supporting Information is available free of charge at https://pubs.acs.org/doi/10.1021/acsami.2c22371.

Supplementary materials and methods, fabrication steps of the tendon-on-CNC-chip models (Figure S1), rheological characterization of PL solutions and hydrogels (Figure S2), and a table of primer sequences for RT-PCR (Table S1) (PDF)

Movie S1 of the first 9 days of the culture of multicellular constructs, showing the migration of endothelial cells toward the tendon compartment (scale bar: 500 μm) (MP4)

Movie S2 of days 7−9 of the culture of multicellular constructs, showing the migration of endothelial cells toward the tendon compartment (scale bar: 500 μm) (AVI)

https://doi.org/10.1021/acsami.2c22371
ACS Appl. Mater. Interfaces 2023, 15, 50598−50611

AUTHOR INFORMATION

Corresponding Authors

Rui M. A. Domingues − *3B's Research Group, I3Bs—Research Institute on Biomaterials, Biodegradables and Biomimetics, University of Minho, Headquarters of the European Institute of Excellence on Tissue Engineering and Regenerative Medicine, 4805-017 Barco, Guimarães, Portugal; ICVS/3B's—PT Government Associate Laboratory, 4800 Braga/Guimarães, Portugal;* orcid.org/0000-0002-3654-9906; Email: rui.domingues@i3bs.uminho.pt

Manuela E. Gomes − *3B's Research Group, I3Bs—Research Institute on Biomaterials, Biodegradables and Biomimetics, University of Minho, Headquarters of the European Institute of Excellence on Tissue Engineering and Regenerative Medicine, 4805-017 Barco, Guimarães, Portugal; ICVS/3B's—PT Government Associate Laboratory, 4800 Braga/Guimarães, Portugal;* orcid.org/0000-0002-2036-6291; Email: megomes@i3bs.uminho.pt

Authors

Rosa F. Monteiro − *3B's Research Group, I3Bs—Research Institute on Biomaterials, Biodegradables and Biomimetics, University of Minho, Headquarters of the European Institute of Excellence on Tissue Engineering and Regenerative Medicine, 4805-017 Barco, Guimarães, Portugal; ICVS/3B's—PT Government Associate Laboratory, 4800 Braga/Guimarães, Portugal*

Syeda M. Bakht − *3B's Research Group, I3Bs—Research Institute on Biomaterials, Biodegradables and Biomimetics, University of Minho, Headquarters of the European Institute of Excellence on Tissue Engineering and Regenerative Medicine, 4805-017 Barco, Guimarães, Portugal; ICVS/3B's—PT Government Associate Laboratory, 4800 Braga/Guimarães, Portugal*

Manuel Gomez-Florit − *3B's Research Group, I3Bs—Research Institute on Biomaterials, Biodegradables and Biomimetics, University of Minho, Headquarters of the European Institute of Excellence on Tissue Engineering and Regenerative Medicine, 4805-017 Barco, Guimarães, Portugal; ICVS/3B's—PT Government Associate Laboratory, 4800 Braga/Guimarães, Portugal*

Fernanda C. Stievani − *Department of Veterinary Surgery and Animal Reproduction, Regenerative Medicine Laboratory, School of Veterinary Medicine and Animal Science, São Paulo State University (UNESP), 18607-400 Botucatu, Brazil*

Ana L. G. Alves − *Department of Veterinary Surgery and Animal Reproduction, Regenerative Medicine Laboratory, School of Veterinary Medicine and Animal Science, São Paulo State University (UNESP), 18607-400 Botucatu, Brazil*

Rui L. Reis − *3B's Research Group, I3Bs—Research Institute on Biomaterials, Biodegradables and Biomimetics, University of Minho, Headquarters of the European Institute of Excellence on Tissue Engineering and Regenerative Medicine, 4805-017 Barco, Guimarães, Portugal; ICVS/3B's—PT Government Associate Laboratory, 4800 Braga/Guimarães, Portugal*

Complete contact information is available at: https://pubs.acs.org/10.1021/acsami.2c22371

Notes

The authors declare no competing financial interest.

ACKNOWLEDGMENTS

The authors thank Hospital da Prelada (Porto, Portugal) for providing adipose tissue samples. The authors acknowledge the financial support from Project NORTE-01-0145-FEDER 000021 supported by Norte Portugal Regional Operational Program (NORTE 2020), under the PORTUGAL 2020 Partnership Agreement, through the European Regional Development Fund (ERDF), the European Union Framework Program for Research and Innovation HORIZON 2020, under the Twinning Grant Agreement 810850-Achilles, and European Research Council Grant Agreement 772817 and 101069302, Fundação para a Ciência e a Tecnologia for the Ph.D. grant PD/BD/129403/2017 (to S.M.B.) financed through the doctoral program in Tissue Engineering, Regenerative Medicine and Stem Cells (TERM&SC), for Contract 2020.03410.CEECIND and 2022.05526.PTDC (to R.M.A.D.). The authors acknowledge Doctor Alberto Pardo for performing the rheology measurements of the PL bioink. The schematics in Figures [1], [2]A, [4]A, and [6]A and Table of Contents graphic were created with BioRender.com.

REFERENCES

(1) Stauber, T.; Wolleb, M.; Duss, A.; Jaeger, P. K.; Heggli, I.; Hussien, A. A.; Blache, U.; Snedeker, J. G. Extrinsic Macrophages Protect While Tendon Progenitors Degrade: Insights from a Tissue Engineered Model of Tendon Compartmental Crosstalk. *Adv. Healthc. Mater.* **2021**, *10* (20), 2100741.

(2) Lee, C. Tendon Physiology and Repair. *Orthop. Trauma* **2021**, *35* (5), 274−281.

(3) Docheva, D.; Müller, S. A.; Majewski, M.; Evans, C. H. Biologics for Tendon Repair. *Adv. Drug Delivery Rev.* **2015**, *84*, 222−239.

(4) Gomez-Florit, M.; Labrador-Rached, C. J.; Domingues, R. M. A.; Gomes, M. E. The Tendon Microenvironment: Engineered In Vitro Models to Study Cellular Crosstalk. *Adv. Drug Delivery Rev.* **2022**, *185*, 114299.

(5) Snedeker, J. G.; Foolen, J. Tendon Injury and Repair − A Perspective on the Basic Mechanisms of Tendon Disease and Future Clinical Therapy. *Acta Biomater* **2017**, *63*, 18−36.

(6) Millar, N. L.; Silbernagel, K. G.; Thorborg, K.; Kirwan, P. D.; Galatz, L. M.; Abrams, G. D.; Murrell, G. A. C.; McInnes, I. B.; Rodeo, S. A. Tendinopathy. *Nat. Rev. Dis. Prim.* **2021**, *7* (1), 1.

(7) Freedman, B. R.; Mooney, D. J.; Weber, E. Advances toward Transformative Therapies for Tendon Diseases. *Sci. Transl. Med.* **2022**, *14* (661), No. eabl8814.

(8) Wunderli, S. L.; Blache, U.; Snedeker, J. G. Tendon Explant Models for Physiologically Relevant in Vitro Study of Tissue Biology − a Perspective Biology − a Perspective. *Connect. Tissue Res.* **2020**, *61* (3−4), 262−277.

(9) Ribitsch, I.; Baptista, P. M.; Lange-Consiglio, A.; Melotti, L.; Patruno, M.; Jenner, F.; Schnabl-Feichter, E.; Dutton, L. C.; Connolly, D. J.; van Steenbeek, F. G.; Dudhia, J.; Penning, L. C. Large Animal Models in Regenerative Medicine and Tissue Engineering: To Do or Not to Do. *Front. Bioeng. Biotechnol.* **2020**, *8*. DOI: 10.3389/fbioe.2020.00972.

(10) Oreff, G. L.; Fenu, M.; Vogl, C.; Ribitsch, I.; Jenner, F. Species Variations in Tenocytes' Response to Inflammation Require Careful Selection of Animal Models for Tendon Research. *Sci. Rep.* **2021**, *11* (1), 12451.

(11) Yao, L.; Bestwick, C. S.; Bestwick, L. A.; Maffulli, N.; Aspden, R. M. Phenotypic Drift in Human Tenocyte Culture. *Tissue Eng.* **2006**, *12* (7), 1843−1849.

(12) Parrish, J.; Lim, K.; Zhang, B.; Radisic, M.; Woodfield, T. B. F. New Frontiers for Biofabrication and Bioreactor Design in Microphysiological System Development. *Trends Biotechnol* **2019**, *37* (12), 1327−1343.

(13) Calejo, I.; Labrador-Rached, C. J.; Gomez-Florit, M.; Docheva, D.; Reis, R. L.; Domingues, R. M. A.; Gomes, M. E. Bioengineered 3D Living Fibers as In Vitro Human Tissue Models of Tendon Physiology and Pathology. *Adv. Healthc. Mater.* **2022**, *11* (15), 2102863.
(14) Mehta, V.; Rath, S. N. 3D Printed Microfluidic Devices: A Review Focused on Four Fundamental Manufacturing Approaches and Implications on the Field of Healthcare. *Bio-Design Manuf.* **2021**, *4* (2), 311−343.
(15) Ingber, D. E. Human Organs-on-Chips for Disease Modelling, Drug Development and Personalized Medicine. *Nat. Rev. Genet.* **2022**, *23* (8), 467−491.
(16) Piluso, S.; Li, Y.; Abinzano, F.; Levato, R.; Moreira Teixeira, L.; Karperien, M.; Leijten, J.; van Weeren, R.; Malda, J. Mimicking the Articular Joint with In Vitro Models. *Trends Biotechnol* **2019**, *37* (10), 1063−1077.
(17) Campbell, S. B.; Wu, Q.; Yazbeck, J.; Liu, C.; Okhovatian, S.; Radisic, M. Beyond Polydimethylsiloxane: Alternative Materials for Fabrication of Organ-on-a-Chip Devices and Microphysiological Systems. *ACS Biomater. Sci. Eng.* **2021**, *7* (7), 2880−2899.
(18) Mota, C.; Camarero-Espinosa, S.; Baker, M. B.; Wieringa, P.; Moroni, L. Bioprinting: From Tissue and Organ Development to in Vitro Models. *Chem. Rev.* **2020**, *120* (19), 10547−10607.
(19) Levato, R.; Jungst, T.; Scheuring, R. G.; Blunk, T.; Groll, J.; Malda, J. From Shape to Function: The Next Step in Bioprinting. *Adv. Mater.* **2020**, *32* (12), 1906423.
(20) McCormack, A.; Highley, C. B.; Leslie, N. R.; Melchels, F. P. W. 3D Printing in Suspension Baths: Keeping the Promises of Bioprinting Afloat. *Trends Biotechnol* **2020**, *38* (6), 584−593.
(21) Kajtez, J.; Wesseler, M. F.; Birtele, M.; Khorasgani, F. R.; Rylander Ottosson, D.; Heiskanen, A.; Kamperman, T.; Leijten, J.; Martínez-Serrano, A.; Larsen, N. B.; Angelini, T. E.; Parmar, M.; Lind, J. U.; Emnéus, J. Embedded 3D Printing in Self-Healing Annealable Composites for Precise Patterning of Functionally Mature Human Neural Constructs. *Adv. Sci.* **2022**, *9*, 2201392.
(22) Daly, A. C.; Davidson, M. D.; Burdick, J. A. 3D Bioprinting of High Cell-Density Heterogeneous Tissue Models through Spheroid Fusion within Self-Healing Hydrogels. *Nat. Commun.* **2021**, *12* (1), 753.
(23) Bakht, S. M.; Gomez-Florit, M.; Lamers, T.; Reis, R. L.; Domingues, R. M. A.; Gomes, M. E. 3D Bioprinting of Miniaturized Tissues Embedded in Self-Assembled Nanoparticle-Based Fibrillar Platforms. *Adv. Funct. Mater.* **2021**, *31* (46), 2104245.
(24) Antich, C.; de Vicente, J.; Jiménez, G.; Chocarro, C.; Carrillo, E.; Montañez, E.; Gálvez-Martín, P.; Marchal, J. A. Bio-Inspired Hydrogel Composed of Hyaluronic Acid and Alginate as a Potential Bioink for 3D Bioprinting of Articular Cartilage Engineering Constructs. *Acta Biomater* **2020**, *106*, 114−123.
(25) Petta, D.; D'Amora, U.; Ambrosio, L.; Grijpma, D. W.; Eglin, D.; D'Este, M. Hyaluronic Acid as a Bioink for Extrusion-Based 3D Printing. *Biofabrication* **2020**, *12* (3), 32001.
(26) Leucht, A.; Volz, A.-C.; Rogal, J.; Borchers, K.; Kluger, P. J. Advanced Gelatin-Based Vascularization Bioinks for Extrusion-Based Bioprinting of Vascularized Bone Equivalents. *Sci. Rep.* **2020**, *10* (1), 5330.
(27) Bernal, P. N.; Bouwmeester, M.; Madrid-Wolff, J.; Falandt, M.; Florczak, S.; Rodriguez, N. G.; Li, Y.; Größbacher, G.; Samsom, R.; van Wolferen, M.; van der Laan, L. J. W.; Delrot, P.; Loterie, D.; Malda, J.; Moser, C.; Spee, B.; Levato, R. Volumetric Bioprinting of Organoids and Optically Tuned Hydrogels to Build Liver-Like Metabolic Biofactories. *Adv. Mater.* **2022**, *34* (15), 2110054.
(28) Diamantides, N.; Dugopolski, C.; Blahut, E.; Kennedy, S.; Bonassar, L. J. High Density Cell Seeding Affects the Rheology and Printability of Collagen Bioinks. *Biofabrication* **2019**, *11* (4), 45016.
(29) Kim, B. S.; Das, S.; Jang, J.; Cho, D.-W. Decellularized Extracellular Matrix-Based Bioinks for Engineering Tissue- and Organ-Specific Microenvironments. *Chem. Rev.* **2020**, *120* (19), 10608−10661.
(30) Kang, B.; Park, Y.; Hwang, D. G.; Kim, D.; Yong, U.; Lim, K. S.; Jang, J. Facile Bioprinting Process for Fabricating Size-Controllable Functional Microtissues Using Light-Activated Decellularized Extracellular Matrix-Based Bioinks. *Adv. Mater. Technol.* **2022**, *7*, 2100947.
(31) Zhao, F.; Cheng, J.; Zhang, J.; Yu, H.; Dai, W.; Yan, W.; Sun, M.; Ding, G.; Li, Q.; Meng, Q.; Liu, Q.; Duan, X.; Hu, X.; Ao, Y. Comparison of Three Different Acidic Solutions in Tendon Decellularized Extracellular Matrix Bio-Ink Fabrication for 3D Cell Printing. *Acta Biomater* **2021**, *131* (xxxx), 262−275.
(32) Chae, S.; Sun, Y.; Choi, Y.-J.; Ha, D.-H.; Jeon, I.; Cho, D.-W. 3D Cell-Printing of Tendon-Bone Interface Using Tissue-Derived Extracellular Matrix Bioinks for Chronic Rotator Cuff Repair. *Biofabrication* **2021**, *13* (3), 035005.
(33) Zhao, F.; Cheng, J.; Sun, M.; Yu, H.; Wu, N.; Li, Z.; Zhang, J.; Li, Q.; Yang, P.; Liu, Q.; Hu, X.; Ao, Y. Digestion Degree Is a Key Factor to Regulate the Printability of Pure Tendon Decellularized Extracellular Matrix Bio-Ink in Extrusion-Based 3D Cell Printing. *Biofabrication* **2020**, *12* (4), 045011.
(34) Liu, W.; Wang, B.; Cao, Y. Engineered Tendon Repair and Regeneration. In *Tendon Regeneration*; Gomes, M. E., Reis, R. L., Rodrigues, M. T. B. T.-T. R., Eds.; Elsevier: Boston, MA, 2015; pp 381−412. DOI: 10.1016/B978-0-12-801590-2.00014-4.
(35) Gonçalves, A. I.; Costa-Almeida, R.; Gershovich, P.; Rodrigues, M. T.; Reis, R. L.; Gomes, M. E. Cell-Based Approaches for Tendon Regeneration. In *Tendon Regeneration*; Gomes, M. E., Reis, R. L., Rodrigues, M. T. B. T.-T. R., Eds.; Elsevier: Boston, MA, 2015; pp 187−203. DOI: 10.1016/B978-0-12-801590-2.00006-5.
(36) Hirpara, K. M.; Abouazza, O.; O'Neill, B.; O'Sullivan, M. A TECHNIQUE FOR PORCINE FLEXOR TENDON HARVEST. *J. Musculoskelet. Res.* **2006**, *10* (04), 181−186.
(37) Toprakhisar, B.; Nadernezhad, A.; Bakirci, E.; Khani, N.; Skvortsov, G. A.; Koc, B. Development of Bioink from Decellularized Tendon Extracellular Matrix for 3D Bioprinting. *Macromol. Biosci.* **2018**, *18* (10), 1800024.
(38) Farnebo, S.; Woon, C. Y. L.; Schmitt, T.; Joubert, L.-M.; Kim, M.; Pham, H.; Chang, J. Design and Characterization of an Injectable Tendon Hydrogel: A Novel Scaffold for Guided Tissue Regeneration in the Musculoskeletal System. *Tissue Eng. Part A* **2014**, *20* (9−10), 1550−1561.
(39) Bondeson, D.; Mathew, A.; Oksman, K. Optimization of the Isolation of Nanocrystals from Microcrystalline Cellulose by Acid Hydrolysis. *Cellulose* **2006**, *13* (2), 171−180.
(40) Carvalho, P. P.; Wu, X.; Yu, G.; Dias, I. R.; Gomes, M. E.; Reis, R. L.; Gimble, J. M. The Effect of Storage Time on Adipose-Derived Stem Cell Recovery from Human Lipoaspirates. *Cells Tissues Organs* **2011**, *194* (6), 494−500.
(41) Mendes, B. B.; Gómez-Florit, M.; Hamilton, A. G.; Detamore, M. S.; Domingues, R. M. A.; Reis, R. L.; Gomes, M. E. Human Platelet Lysate-Based Nanocomposite Bioink for Bioprinting Hierarchical Fibrillar Structures. *Biofabrication* **2020**, *12* (1), 015012.
(42) Badylak, S. F. Xenogeneic Extracellular Matrix as a Scaffold for Tissue Reconstruction. *Transpl. Immunol.* **2004**, *12* (3), 367−377.
(43) Crapo, P. M.; Gilbert, T. W.; Badylak, S. F. An Overview of Tissue and Whole Organ Decellularization Processes. *Biomaterials* **2011**, *32* (12), 3233−3243.
(44) Vernengo, A. J.; Grad, S.; Eglin, D.; Alini, M.; Li, Z. Bioprinting Tissue Analogues with Decellularized Extracellular Matrix Bioink for Regeneration and Tissue Models of Cartilage and Intervertebral Discs. *Adv Funct Mater* **2020**, *30*, 1909044.
(45) Fernández-Pérez, J.; Ahearne, M. The Impact of Decellularization Methods on Extracellular Matrix Derived Hydrogels. *Sci. Rep.* **2019**, *9* (1), 14933.
(46) Puetzer, J. L.; Ma, T.; Sallent, I.; Gelmi, A.; Stevens, M. M. Driving Hierarchical Collagen Fiber Formation for Functional Tendon, Ligament, and Meniscus Replacement. *Biomaterials* **2021**, *269*, 120527.
(47) Cooke, M. E.; Rosenzweig, D. H. The Rheology of Direct and Suspended Extrusion Bioprinting. *APL Bioeng* **2021**, *5* (1), 011502.

(48) Jang, J.; Park, J. Y.; Gao, G.; Cho, D.-W. Biomaterials-Based 3D Cell Printing for next-Generation Therapeutics and Diagnostics. *Biomaterials* **2018**, *156*, 88−106.
(49) Zhang, J.; Wang, J. H.-C. Human Tendon Stem Cells Better Maintain Their Stemness in Hypoxic Culture Conditions. *PLoS One* **2013**, *8* (4), No. e61424.
(50) Zhao, Y.; Rafatian, N.; Wang, E. Y.; Feric, N. T.; Lai, B. F. L.; Knee-Walden, E. J.; Backx, P. H.; Radisic, M. Engineering Microenvironment for Human Cardiac Tissue Assembly in Heart-on-a-Chip Platform. *Matrix Biol.* **2020**, *85*−*86*, 189−204.
(51) Zhang, B.; Korolj, A.; Lai, B. F. L.; Radisic, M. Advances in Organ-on-a-Chip Engineering. *Nat. Rev. Mater.* **2018**, *3* (8), 257−278.
(52) Jones, D. L.; Daniels, R. N.; Jiang, X.; Locke, R. C.; Evans, M. K.; Bonnevie, E. D.; Srikumar, A.; Nijsure, M. P.; Boerckel, J. D.; Mauck, R. L.; Dyment, N. A. Mechano-Epigenetic Regulation of Extracellular Matrix Homeostasis via Yap and Taz. *bioRxiv* **2022**, DOI: 10.1101/2022.07.11.499650.
(53) Meeremans, M.; Van de Walle, G. R.; Van Vlierberghe, S.; De Schauwer, C. The Lack of a Representative Tendinopathy Model Hampers Fundamental Mesenchymal Stem Cell Research. *Front. cell Dev. Biol.* **2021**, *9*, 651164.
(54) Laranjeira, M.; Domingues, R. M. A.; Costa-Almeida, R.; Reis, R. L.; Gomes, M. E. 3D Mimicry of Native-Tissue-Fiber Architecture Guides Tendon-Derived Cells and Adipose Stem Cells into Artificial Tendon Constructs. *Small* **2017**, *13* (31), 1700689.
(55) Youngstrom, D. W.; LaDow, J. E.; Barrett, J. G. Tenogenesis of Bone Marrow-, Adipose-, and Tendon-Derived Stem Cells in a Dynamic Bioreactor. *Connect. Tissue Res.* **2016**, *57* (6), 454−465.
(56) Dede Eren, A.; Sinha, R.; Eren, E. D.; Huipin, Y.; Gulce-Iz, S.; Valster, H.; Moroni, L.; Foolen, J.; de Boer, J. Decellularized Porcine Achilles Tendon Induces Anti-Inflammatory Macrophage Phenotype In Vitro and Tendon Repair In Vivo. *J. Immunol. Regen. Med.* **2020**, *8*, 100027.
(57) Schneider, M.; Angele, P.; Järvinen, T. A. H.; Docheva, D. Rescue Plan for Achilles: Therapeutics Steering the Fate and Functions of Stem Cells in Tendon Wound Healing. *Adv. Drug Delivery Rev.* **2018**, *129*, 352−375.
(58) Shukunami, C.; Takimoto, A.; Oro, M.; Hiraki, Y. Scleraxis Positively Regulates the Expression of Tenomodulin, a Differentiation Marker of Tenocytes. *Dev. Biol.* **2006**, *298* (1), 234−247.
(59) Almeida, H.; Domingues, R. M. A.; Mithieux, S. M.; Pires, R. A.; Gonçalves, A. I.; Gómez-Florit, M.; Reis, R. L.; Weiss, A. S.; Gomes, M. E. Tropoelastin-Coated Tendon Biomimetic Scaffolds Promote Stem Cell Tenogenic Commitment and Deposition of Elastin-Rich Matrix. *ACS Appl. Mater. Interfaces* **2019**, *11* (22), 19830−19840.
(60) Maffulli, N.; Renström, P.; Leadbetter, W. B. *Tendon Injuries*; Maffulli, N., Renström, P., Leadbetter, W. B., Eds.; Springer-Verlag: London, 2005. DOI: 10.1007/b137778.
(61) Tempfer, H.; Traweger, A. Tendon Vasculature in Health and Disease. *Front. Physiol.* **2015**, *6*. DOI: 10.3389/fphys.2015.00330.
(62) Santo, V. E.; Duarte, A. R. C.; Popa, E. G.; Gomes, M. E.; Mano, J. F.; Reis, R. L. Enhancement of Osteogenic Differentiation of Human Adipose Derived Stem Cells by the Controlled Release of Platelet Lysates from Hybrid Scaffolds Produced by Supercritical Fluid Foaming. *J. Controlled Release* **2012**, *162* (1), 19−27.
(63) Mendes, B. B.; Gómez-Florit, M.; Babo, P. S.; Domingues, R. M.; Reis, R. L.; Gomes, M. E. Blood Derivatives Awaken in Regenerative Medicine Strategies to Modulate Wound Healing. *Adv. Drug Delivery Rev.* **2018**, *129*, 376−393.
(64) Mendes, B. B.; Gómez-Florit, M.; Pires, R. A.; Domingues, R. M. A.; Reis, R. L.; Gomes, M. E. Human-Based Fibrillar Nanocomposite Hydrogels as Bioinstructive Matrices to Tune Stem Cell Behavior. *Nanoscale* **2018**, *10* (36), 17388−17401.
(65) Fortunato, T. M.; Beltrami, C.; Emanueli, C.; De Bank, P. A.; Pula, G. Platelet Lysate Gel and Endothelial Progenitors Stimulate Microvascular Network Formation in Vitro: Tissue Engineering Implications. *Sci. Rep.* **2016**, *6* (April), 1−15.
(66) Robinson, S. T.; Douglas, A. M.; Chadid, T.; Kuo, K.; Rajabalan, A.; Li, H.; Copland, I. B.; Barker, T. H.; Galipeau, J.; Brewster, L. P. A Novel Platelet Lysate Hydrogel for Endothelial Cell and Mesenchymal Stem Cell-Directed Neovascularization. *Acta Biomater* **2016**, *36*, 86−98.
(67) Liu, X.; Zhu, B.; Li, Y.; Liu, X.; Guo, S.; Wang, C.; Li, S.; Wang, D. The Role of Vascular Endothelial Growth Factor in Tendon Healing. *Front. Physiol.* **2021**, *12*, 766080.
(68) Lai, F.; Wang, J.; Tang, H.; Huang, P.; Liu, J.; He, G.; Zhou, M.; Tao, X.; Tang, K. VEGF Promotes Tendon Regeneration of Aged Rats by Inhibiting Adipogenic Differentiation of Tendon Stem/Progenitor Cells and Promoting Vascularization. *FASEB J.* **2022**, *36* (8), No. e22433.
(69) Wu, S.; Wang, Y.; Streubel, P. N.; Duan, B. Living Nanofiber Yarn-Based Woven Biotextiles for Tendon Tissue Engineering Using Cell Tri-Culture and Mechanical Stimulation. *Acta Biomater* **2017**, *62*, 102−115.
(70) Rothrauff, B. B.; Yang, G.; Tuan, R. S. Tendon Resident Cells—Functions and Features in Section I—Developmental Biology and Physiology of Tendons. In *Tendon Regeneration*; Elsevier, 2015; pp 41−76. DOI: 10.1016/B978-0-12-801590-2.00002-8.
(71) Millar, N. L.; Murrell, G. A. C.; Mcinnes, I. B. Inflammatory Mechanisms in Tendinopathy − towards Translation. *Nat. Rev. Rheumatol.* **2017**, *13* (2), 110−122.
(72) Dean, B. J. F.; Dakin, S. G.; Millar, N. L.; Carr, A. J. Review: Emerging Concepts in the Pathogenesis of Tendinopathy. *The Surgeon* **2017**, *15* (6), 349−354.